Supplemental Materials

On the modeling of graphene layer by a thin dielectric

Modeling graphene as a 2D surface having an appropriate value of surface conductivity σ is an accurate approach for a semiclassical analysis (e.g., the Drude model for intraband contributions has been verified experimentally,[1–3] and the interband model and the visible-spectrum response have also been verified[3]). However, often it is convenient to model graphene as a thin dielectric layer, which is easily implemented in typical electromagnetic simulation codes. It is common to consider an equivalent dielectric slab with the thickness of d and a 3D conductivity of $\sigma_{3D} = \sigma/d$. The corresponding bulk (3D) relative permittivity is[4]

$$\varepsilon_{3D} = 1 + \frac{\sigma}{j\omega\varepsilon_0 d}, \qquad (S.1)$$

where ω is the angular frequency. However, for calculations in which the geometry is discretized (e.g., in the finite-element method), fine features in the geometry such as an electrically-thin slab demand finer discretization, which in turn requires more computational costs. Thus, whereas sub 1 nm thickness values may seem more physically-appropriate, numerical considerations often lead to the use of a thicker material. As an example, in Ref.[4] the thickness of the dielectric slab is assumed to be 1 nm.

However, the accuracy of the dielectric model degrades as the thickness of the slab increases. Since this model is widely adopted, yet a detailed consideration of this effect has not been previously presented, we briefly consider this topic below.

Consider a transverse magnetic SPP on an infinite graphene layer. The SPP wavelength using the 2D conductivity is[5]

$$\lambda_{SPP} = \lambda_0 \left(1 - \left(\frac{2}{\eta_0\sigma}\right)^2\right)^{-0.5}, \qquad (S.2)$$

where λ_0 is the wavelength in free space. On the other hand, in Ref.[6] it is shown that a dielectric slab with negative permittivity ambient in a medium with positive permittivity can support two sets of dielectric modes (even and odd). The odd modes have the wavelength (assuming vacuum as the ambient medium)

$$\lambda_{odd} = 2\pi \left(-\frac{2}{d}\coth^{-1}\varepsilon_{3D}\right)^{-1}, \qquad (S.3)$$

where ε_{3D} and d are the dielectric slab permittivity and thickness, respectively. It is shown in Ref.[6] that the odd modes can exist only if

$$\varepsilon_{3D} < -1. \qquad (S.4)$$

It can also be noticed that the modal field distribution outside of the slab is similar to that of a SPP on graphene. It is easy to show that in the limit of $d \to 0$ and using (S.1), the dielectric-slab odd mode becomes the graphene SPP mode $\lambda_{odd} \to \lambda_{SPP}$. It can be shown that (S.3) is a good approximation for λ_{SPP} only if three conditions are satisfied as [see the next sub-section]

$$\frac{d}{\lambda_{SPP}} \ll 1, \qquad (S.5)$$

$$|\sigma| \ll \frac{2}{\eta_0}, \qquad (S.6)$$

$$\left|\frac{\sigma}{d}\right| > 2\omega\varepsilon_0. \qquad (S.7)$$

Equation (S.7) is in fact the direct insertion of (S.1) into (S.4). Based on (S.7), as the σ/d ra-

tio increases, the dielectric slab becomes a better approximation (as long as (S.6) is not violated). To consider this, Fig. S.1 shows the frequency independent error (%) of using the dielectric slab model for graphene as a function of the normalized d and σ (assuming σ is imaginary-valued),

$$\text{error}(\%) = \frac{\lambda_{\text{odd}} - \lambda_{\text{SPP}}}{\lambda_{\text{SPP}}} \times 100. \qquad \text{(S.8)}$$
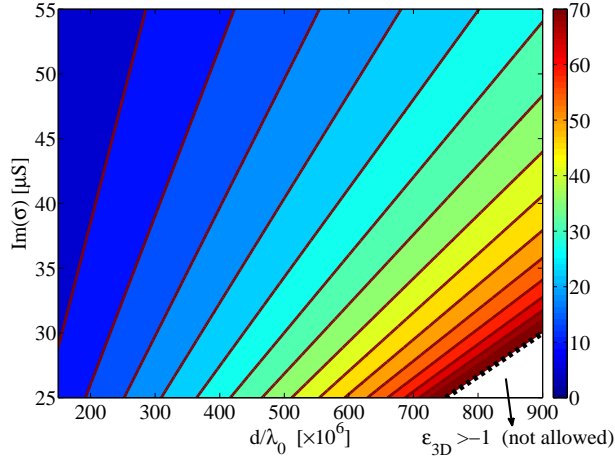

Figure S.1: The error (S.8) as a function of the normalized dielectric thickness and conductivity of graphene. The graph is frequency independent.

As a numerical example (using equations (3) and (4) in Ref.[5]), for $d = 2\,\text{nm}$, the scattering rate $\Gamma = 0.215\,\text{meV}$, and chemical potential $\mu_c = 0.03\,\text{eV}$ at $f = 10\,\text{THz}$ and very low temperature ($T = 3\,\text{K}$), the normalized thickness and conductivity will be $d/\lambda_0 = 66.7 \times 10^{-6}$ and $\sigma = 1.1 - j23\,\mu\text{S}$ which leads to an error of 4.9%. This is set as the maximum error that is allowed in the rest of this work.

Proof of (S.7)

From (S.3),

$$\coth\left(\frac{d\,|\beta_{\text{odd}}|}{2}\right) = \frac{\sigma^i}{\omega\varepsilon_0 d} - 1 \qquad \text{(S.9)}$$

where $\beta_{\text{odd}} = 2\pi/\lambda_{\text{odd}}$ and $\sigma = -j\sigma^i$.

Assuming $d/\lambda_{\text{odd}} \ll 1$, (S.9) leads to

$$\frac{2}{d\,|\beta_{\text{odd}}|} + \frac{d\,|\beta_{\text{odd}}|}{6} - ... = \frac{\sigma^i}{\omega\varepsilon_0 d} - 1. \qquad \text{(S.10)}$$

After keeping only the first term of the series in (S.10) and using the assumption $d/\lambda_{\text{odd}} \ll 1$,

$$\frac{|\lambda_{\text{odd}}|}{\lambda_0} = \frac{\sigma^i \eta_0}{2}. \qquad \text{(S.11)}$$

Comparing (S.11) and (S.2), λ_{odd} is a good approximation of λ_{SPP} only if

$$|\sigma^i| \ll \frac{2}{\eta_0}. \qquad \text{(S.12)}$$

Proof of (2)

For the anisotropic region of Fig. 1, consider a general magnetic field in the Fourier transform domain as

$$\mathbf{H} = e^{-jk_y y - jk_z z} \times \qquad \text{(S.13)}$$

$$\begin{cases} \left(H_x^+\hat{\mathbf{x}} + H_y^+\hat{\mathbf{y}} + H_z^+\hat{\mathbf{z}}\right) e^{-\sqrt{k_y^2 + k_z^2 - k_0^2}\,x} & x > 0 \\ \left(H_x^-\hat{\mathbf{x}} + H_y^-\hat{\mathbf{y}} + H_z^-\hat{\mathbf{z}}\right) e^{\sqrt{k_y^2 + k_z^2 - k_0^2}\,x} & x < 0 \end{cases}$$

where $H_{x,y,z}^{+,-}$ are constants. Equation (S.13) is chosen so that it satisfies the Helmholtz equation and has the form of a plasmonic wave.

Using Ampere's law to find the electric field in each region and satisfying the boundary conditions

$$H_y^+ - H_y^- = \sigma_z E_z, \qquad \text{(S.14)}$$

$$H_z^+ - H_z^- = -\sigma_y E_y, \qquad \text{(S.15)}$$

$$H_x^+ = H_x^-, \qquad \text{(S.16)}$$

it is straightforward to show that

$$H_y^- = -H_y^+, \qquad \text{(S.17)}$$

$$H_z^- = -H_z^+, \qquad \text{(S.18)}$$

$$\begin{bmatrix} \sigma_z jk_y & Y & 0 \\ jk_z\sigma_y & 0 & Z \\ k_x & jk_y & jk_z \end{bmatrix} \begin{bmatrix} H_x^+ \\ H_y^+ \\ H_z^+ \end{bmatrix} = 0, \qquad \text{(S.19)}$$

where $Y = -2j\omega\varepsilon_0 - \sigma_z k_x$, and $Z = -2j\omega\varepsilon_0 - k_x\sigma_y$. Setting the determinant of the above matrix
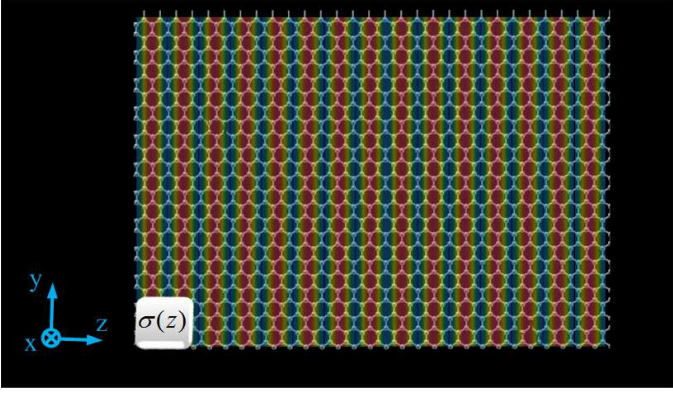
Figure S.2: An infinite graphene layer with isotropic periodic conductivity of $\sigma(z)$.

to zero leads to (2).

It is easy to show that in the isotropic limit ($\sigma_y = \sigma_z = \sigma_0$), (2) simplifies to the well-known dispersion equations[5,7] $k_x = -\frac{2jk_0}{\eta_0\sigma_0}$, and $k_x = -\frac{jk_0\eta_0\sigma_0}{2}$, for transverse magnetic (TM) and transverse electric (TE) surface waves, respectively. The solution of (2) will lead to a solution for the SPP with the magnetic field

$$\mathbf{H} = e^{-k_x x - jk_y y - jk_z z} \times \tag{S.20}$$

$$\left(\hat{\mathbf{x}} + \frac{j\sigma_z k_y}{2j\omega\varepsilon_0 + k_x\sigma_z}\hat{\mathbf{y}} + \frac{j\sigma_y k_z}{2j\omega\varepsilon_0 + k_x\sigma_y}\hat{\mathbf{z}} \right).$$

In the canalization regime, the SPP given by (S.20) is a TM mode with respect to the canalization direction (z-direction in our notation) and its magnetic field has a peculiar circular polarization,

$$\mathbf{H} = (\hat{\mathbf{x}} + j\hat{\mathbf{y}}) e^{-k_y(x+jy) - jk_0 z}. \tag{S.21}$$

It is also interesting that the confinement in the x-direction of each SPP harmonic is proportional to k_y.

Proof of (5) and (6)

Assume a sheet of graphene with a periodic isotropic conductivity in the z-direction ($\sigma(z) = \sigma(z+T)$) as shown in Fig. S.2. Enforcing a constant, uniform, and z-directed surface current (J_z) on the graphene induces an electric field on the graphene as

$$E(z) = \frac{J_z}{\sigma(z)}. \tag{S.22}$$

Defining average parameters leads to

$$E_{\text{av}} = \frac{J_z}{\sigma_{\text{av},z}} = \frac{1}{L}\int\limits_{\langle L \rangle} \frac{J_z}{\sigma(z)}dz, \tag{S.23}$$

$$\frac{1}{\sigma_{\text{av},z}} = \frac{1}{L}\int\limits_{\langle L \rangle} \frac{1}{\sigma(z)}dz. \tag{S.24}$$

Enforcing a constant, uniform and y-directed electric field (E_y) induces a surface current on the graphene as

$$J_y(z) = \sigma(z)E_y \tag{S.25}$$

which is (5).

Defining average parameters leads to

$$J_{y,\text{av}}(z) = \sigma_{\text{av},y}E_y = \frac{1}{L}\int\limits_{\langle L \rangle} \sigma(z)E_y dz, \tag{S.26}$$

$$\sigma_{\text{av},y} = \frac{1}{L}\int\limits_{\langle L \rangle} \sigma(z)dz, \tag{S.27}$$

which is (6).

Idealized graphene nanoribbons with hard-boundaries

An idealization of the modulation scheme discussed in the text would consist of alternating positive and negative imaginary conductivities, with each strip terminating in a sharp transition between positive and negative values (see Fig. S.6). We assume that all of the strips have the same width $W = 4\,\text{nm}$ and conductivity modulus $|\sigma| = 23.5\,\mu\text{S}$, which is the conductivity of a graphene layer for $f = 10\,\text{THz}$, $T = 3\,\text{K}$, $\Gamma = 0.215\,\text{meV}$ and $\mu_c = 0.022\,\text{eV}$ or $\mu_c = 0.03\,\text{eV}$ (for positive and negative $\text{Im}(\sigma)$, respectively). The chemical potential is chosen to minimize the loss at the given frequency. In fact, the ratio $\text{Im}(\sigma)/\text{Re}(\sigma)$ is maximized at this frequency (the ratio is 7 for $\mu_c = 0.022\,\text{eV}$). Since the effect of loss was discussed in the text, here we assume an imaginary-valued conductivity $\sigma = \pm j23.5\,\mu\text{S}$.

3

We refer to this idealized conductivity profile as the hard-boundary case, because of the step discontinuity (sharp transition) of the conductivity between neighboring strips. This resembles the geometry in Ref.[8] for canalization of 3D waves in which there are also hard-boundaries between dielectric slabs with positive and negative permittivites.

As a simulation example of the hard-boundary case, two point sources are placed in front of the source line in Fig. 1 exciting two SPPs on the graphene layer. The point sources are separated by $20\,\mathrm{nm} = 0.15\lambda_{\mathrm{SPP}}$ where $\lambda_{\mathrm{SPP}} = 133\,\mathrm{nm}$ using (S.2), and the canalization area (the region between the source and the image lines) has length $2\lambda_{\mathrm{SPP}} = 250\,\mathrm{nm}$ and width of $100\,\mathrm{nm}$ (which is large compared to the separation between sources). Figure S.3 shows the normalized x-component of the electric field $|E_x|$ at the source line and image line (at the end of the modulated region). Fig. S.4 shows the normalized x-component of the electric field above the surface of the graphene ($x = 5\,\mathrm{nm}$). Note that the region $-1 < x < 1\,\mathrm{nm}$ represents the graphene (since we have used a dielectric slab model for graphene with the thickness of $2\,\mathrm{nm}$).

Canalization is evident from Figs. S.3 and S.4. Figure S.5 shows the normalized field intensities at the source and image lines just above the graphene surface ($x = 1\,\mathrm{nm}$).

Simulation setup for the hard- and the soft-boundary examples

Full-wave simulations have been done using CST Microwave Studio.[CST] In this section we consider the dielectric model of graphene. Figure S.6 shows the simulation setup of the hard-boundary example. The simulation results are given in Figs. S.3-S.5. The graphene strips can be modeled with dielectric slabs having thickness $d = 2\,\mathrm{nm}$ and, using (S.1), permittivities of $\varepsilon^- = -20$ and $\varepsilon^+ = 22$. However, as shown in the insert of Fig. S.6, the permittivity $\varepsilon^+ = 17$ is used rather than $\varepsilon^+ = 22$ because numerical experiments show that that value leads to better canalization. The difference with our analytically-predicted value for best canalization is seemingly because in our analytical
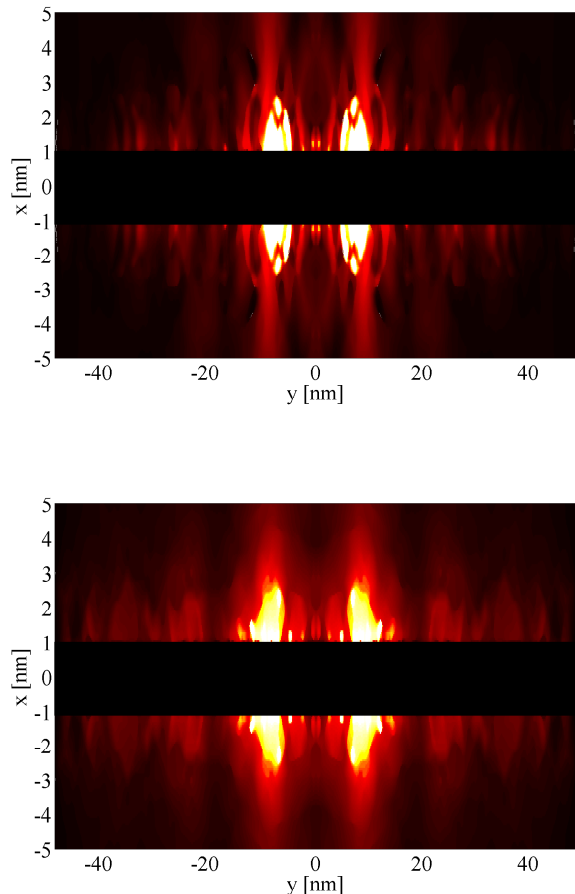

Figure S.3: The normalized x-component of the electric field at the source (top) and image (bottom) planes of the hard-boundary example. Source and image lines are separated by $2\lambda_{\mathrm{SPP}}$ (the region $-1 < x < 1$ is the dielectric slab model of graphene).

model we have disregarded radiation, reflections from discontinuities, and similar effects.

For the soft-boundary example, the conductivity of the strips varies smoothly with position. So, applying the dielectric slab model, we could use a dielectric slab with a fixed thickness (e.g., $d = 2\,\mathrm{nm}$) and a position dependent permittivity given by (S.1) as

$$\varepsilon_{3\mathrm{D}}(z) = 1 + \frac{\sigma(z)}{j\omega\varepsilon_0 d}. \qquad (\text{S.28})$$

However, an alternative method which is easier to implement for simulation is to consider a dielectric slab with fixed permittivity (or permittivities) and a position dependent thickness as
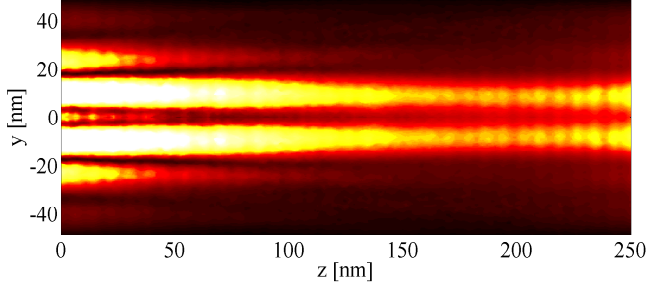
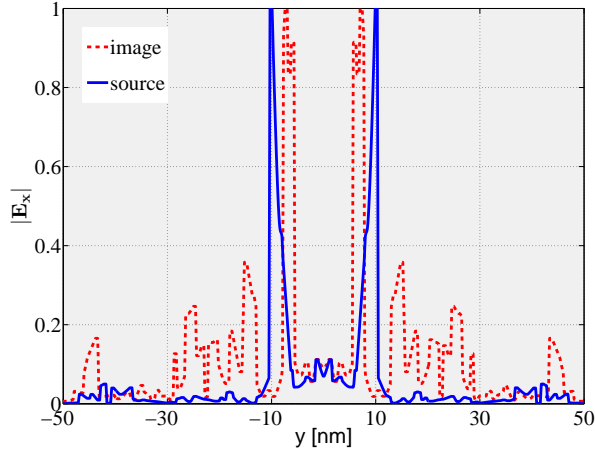Figure S.4: Normalized *x*-component of the electric field above the graphene surface.

Figure S.5: The normalized *x*-components of the electric field at the source and image lines on the surface of the graphene (taken at the height $x = 1\,\mathrm{nm}$) for the hard-boundary example.

$$d(z) = \frac{\sigma(z)}{(\varepsilon_{3D} - 1)\, j\omega\varepsilon_0}. \qquad (S.29)$$

Obviously, two different ε_{3D} values should be chosen for different signs of $\sigma(z)$ so that $d(z)$ remains positive. This has been done for the conductivity of Fig. 3, and the resulting dielectric slab model is shown in Fig. S.7. Comparison between Fig. S.6 and Fig. S.7 clearly shows the difference between the hard- and the soft-boundary examples.
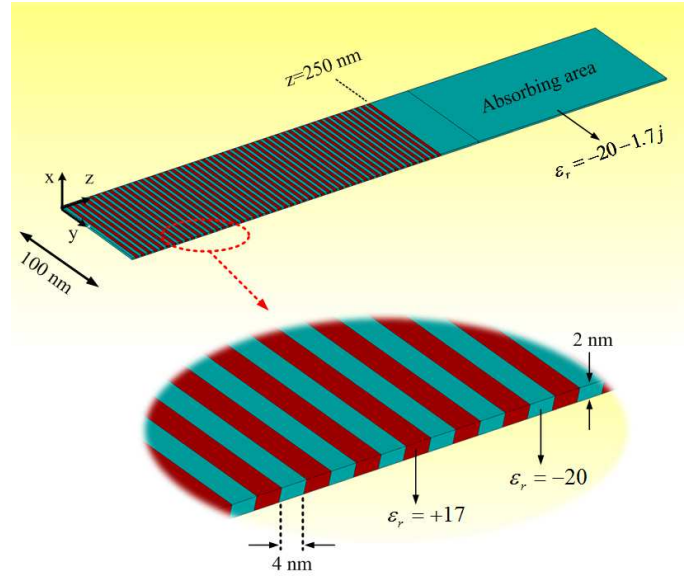
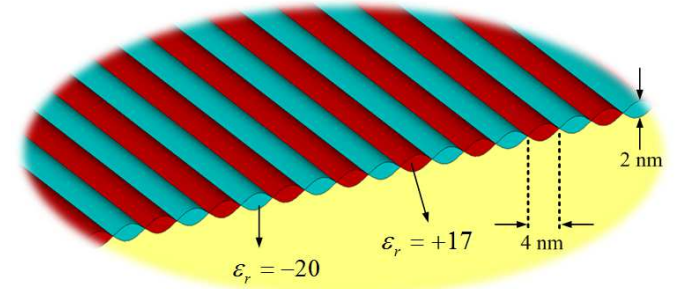Figure S.6: The dielectric model of the hard-boundary graphene strip example.

Figure S.7: The dielectric model for the soft-boundary example - constant permitivies and smoothly-varying thickness model graphene's sinusoidal chemical potential.

The improvement of canalization by increasing the frequency

Figure S.8 shows the ratio Im(σ)/Re(σ) versus chemical potential at three different frequencies, showing that, as frequency increases, loss becomes less important. Note also that the value of chemical potential that maximizes the conductivity ratio is considerably frequency dependent. In Fig. S.9 the effect of decreasing loss as a result of the frequency increase is invesigated. To do so, the peak ratio Im(σ)/Re(σ) of the three curves in Fig. S.8 are chosen associated with frequencies 10, 20, and 30 THz. These ratios are assigned to a same geometry (and holding frequency constant) and the *x*-component of the electric fields are
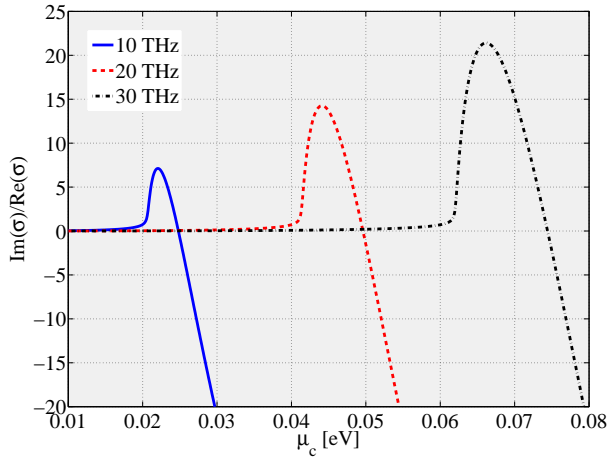
5

Figure S.8: The ratio $\text{Im}(\sigma)/\text{Re}(\sigma)$ as a function of chemical potential for three different frequencies.

shown in Fig. S.9 (the scalings are the same). In this way, all of the electrical lengths (such as the electrical length of the nanoribbons, canalization region, etc.) remain the same and only the effect of loss is incorporated. From Fig. S.9, it is obvious that the increase of frequency improves the canalization. However, since the dimensions become smaller, fabrication becomes more difficult.

Modulated graphene conductivity using a rectangular ridged ground plane

The sinusoidal conductivity of Fig. 3 can be implemented using a rectangular ridged ground plane, as shown in Fig. S.10. The conductivity distribution of the geometry in Fig. S.10 is shown in Fig. S.11 and is almost identical to Fig. 3, although their ground plane geometries are different. Obviously, the ideal canalization behavior of the two geometries is very similar. Interestingly, the rectangular ridged ground plane has to be non-symmetric (the ratio of groove to ridge is 3) to produce the same conductivity function as the symmetrical triangular ridged ground plane.
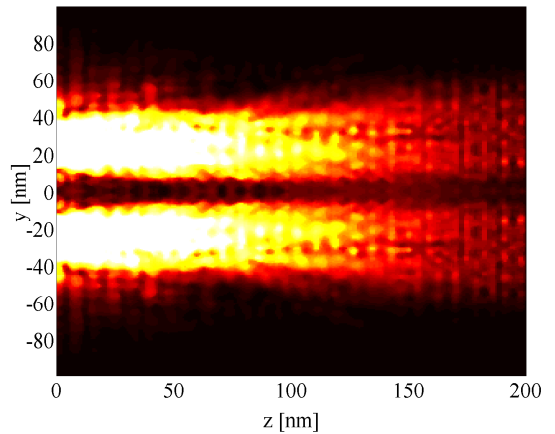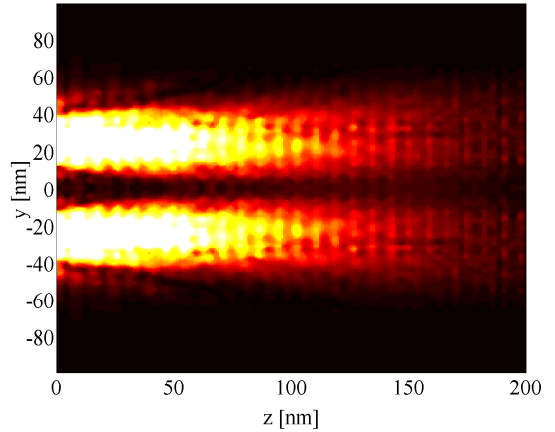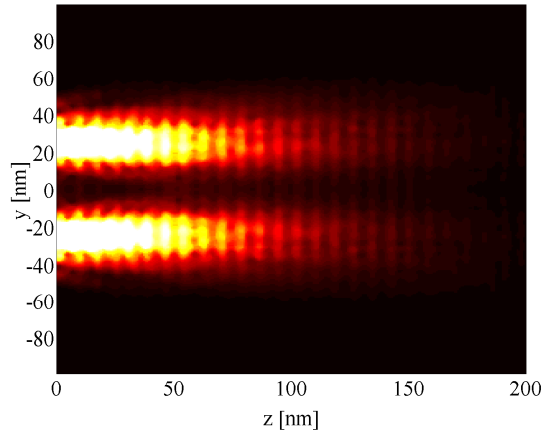
Figure S.9: The normalized x-component of the electric field above the graphene surface ($x = 2\,\text{nm}$) for the peak value of $\text{Im}(\sigma)/\text{Re}(\sigma)$ at 10 THz (top), 20 THz (middle), and 30 THz (bottom).

References

[1] Li, Z. Q.; Henriksen, E. A.; Jiang, Z.; Hao, Z.; Martin, M. C.; Kim, P.; Stormer, H. L.; Basov, D. N. Dirac Charge Dynamics in
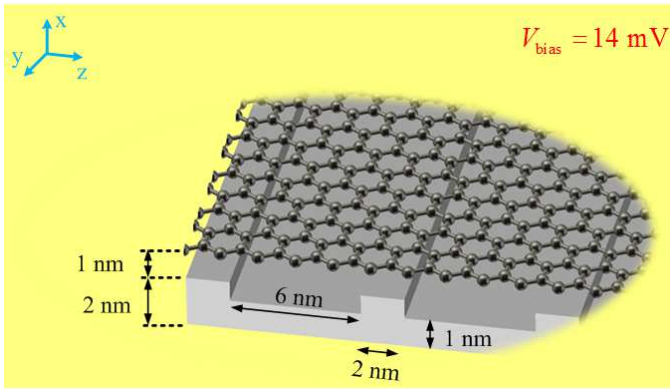
Figure S.10: An alternative geometry with rectangular ridged ground plane to realize the soft-boundary example.
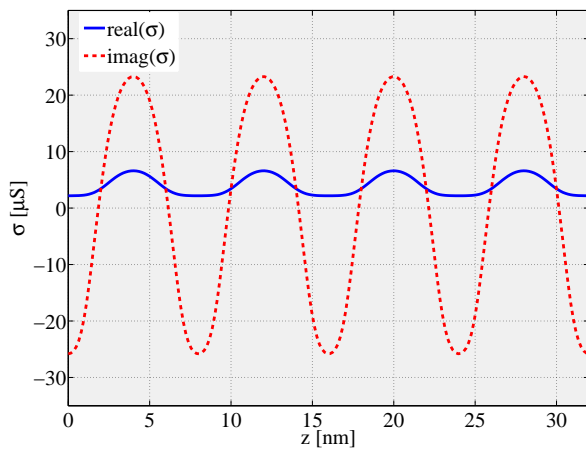

Figure S.11: The conductivity distribution in the geometry of Fig. S.10.

Graphene by Infrared Spectroscopy. *Nat. Phys.* **2008**, *4*, 532–535.

[2] Kim, J. Y.; Lee, C.; Bae, S.; Kim, K. S.; Hong, B. H.; Choi, E. J. Far-Infrared Study of Substrate-Effect on Large Scale Graphene. *Appl. Phys. Lett.* **2011**, *98*, 201907.

[3] Lee, C.; Kim, J. Y.; Bae, S.; Kim, K. S.; Hong, B. H.; Choi, E. J. Optical Response of Large Scale Single Layer Graphene. *Appl. Phys. Lett.* **2011**, *98*, 071905.

[4] Vakil, A.; Engheta, N. Transformation Optics Using Graphene. *Science* **2011**, *332.6035*, 1291–1294.

[5] Hanson, G. W. Dyadic Greens Functions and Guided Surface Waves for a Surface Conduc-tivity Model of Graphene. *J. Appl. Phys.* **2008**, *103*, 064302.

[6] Alù, A.; Engheta, N. Optical Nanotransmis-sion Lines: Synthesis of Planar Left-Handed Metamaterials in the Infrared and Visible Regimes. *JOSA B* **2006**, *23*, 571–583.

[7] Mikhailov, S. A.; Ziegler, K. New Electro-magnetic Mode in Graphene. *Phys. Rev. Lett.* **2007**, *99*, 016803.

[8] Ramakrishna, S. A.; Pendry, J. B.; Wilt-shire, M. C. K.; Stewartar, W. J. Imaging the Near Field. *J. Mod. Opt.* **2003**, *50*, 1419–1430.

[CST] CST Microwave Studio, http://www.cst.com.